Article

Cyclodextrin Metal−Organic Frameworks as a Drug Delivery System for Selected Active Pharmaceutical Ingredients

Kristīne Krūkle-Bērziņa,* Alons Lends, and Anna Boguszewska-Czubara

Read Online

ACCESS | Metrics & More | Article Recommendations | Supporting Information

ABSTRACT: The cyclodextrin-based metal−organic frameworks (CD MOFs) are a suitable molecular platform for drug delivery systems of various active pharmaceutical ingredients (APIs). The low toxicity and cost-efficient synthesis make CD MOFs an attractive host for the encapsulation of APIs. In this study, we created a model system based on γCD-K MOFs with widely used drugs carmofur (HCFU), 5-fluorouracil (5-FU), and salicylic acid (HBA) to study host−guest encapsulation methods using different crystallization protocols. The host−guest complexes of API:CD MOF in an in-depth study were investigated by liquid chromatography−mass spectrometry (LC-MS), differential scanning calorimetry (DSC), thermogravimetric analysis (TGA), and ^{19}F- and ^{13}C-detected solid-state NMR spectroscopy (ssNMR). These techniques confirmed the structure and interaction sites within the encapsulation product in the host−guest complex. We also evaluated the toxicity and biocompatibility of the API:CD MOF complex using *in vitro* and *in vivo* methods. The cytotoxicity, hepatotoxicity, and neurotoxicity were established with cell lines of fibroblasts (BJ), human liver cell line (HepG2), and human oligodendrocytic cells (MO3.13). Then, *Danio rerio* was used as an *in vivo* experimental model of ecotoxicity. The results showed the choice of γCD-K-5 as the most protective and safe option for drug encapsulation to decrease its toxicity level against normal cells.
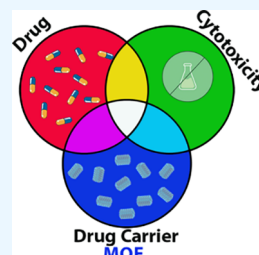
INTRODUCTION

Anticancer drugs have shown significant potential in the targeting and elimination of cancer cells. However, their effectiveness is often hampered by high toxicity to healthy cells.[1] This can lead to severe side effects, impacting the patient's quality of life.[2] Therefore, it is necessary to explore new systems for drug delivery.[3] These delivery systems should be designed to selectively target cancer cells while sparing healthy cells, thereby enhancing the drug's therapeutic efficacy and minimizing its toxic impact on the body.[4]

Therefore, cyclodextrins (CDs) and their derivatives have been intensively studied over the past two decades as drug carriers and other pharmaceuticals. This is related to their ability to improve the stability, solubility, and bioavailability of pharmaceutical active ingredients (APIs).[5]

Metal−organic frameworks (MOFs) have large surface area, well-defined surface properties, and tunable pore sizes.[6] Furthermore, CD-based MOFs have low cytotoxicity, making them viable host matrixes for encapsulating APIs.[7] Numerous studies have been conducted in this field and have attracted an increasing amount of interest in recent years. Notably, drugs like ibuprofen, folic acid, sodium diclofenac, valsartan, and other drugs have been successfully encapsulated in CD-based MOFs using various crystallization protocols, including cocrystallization, vapor diffusion, hydrothermal, and others. These approaches have significantly improved the solubility and bioavailability of the drugs.[8,9]

Carmofur (1-hexylcarbamoyl-5-fluorouracil, HCFU) (Figure 1a) is one of the masked forms of 5-fluorouracil (5-FU, Figure 1b) and has been widely used in the treatment of breast and GI tract carcinomas.[10] Its primary disadvantage is its low solubility in water.[11] 5-FU is a widely used drug for cancer treatment.[12] However, a significant drawback is its tendency to induce drug resistance in tumor cells.[13] Salicylic acid (2-hydroxybenzoic acid (HBA), Figure 1c) is used to treat various skin disorders.[14] Its primary concern is the potential teratogenic risk in the human body,[15] although the cosmetic application of HBA poses no significant risk.[16]

Thus, the scope for the use of HCFU, 5-FU, and HBA in medicine is limited, and there is an urgency to overcome these drawbacks. Previously, several groups have reported encapsulation of 5-FU in different supramolecular host−guest systems.[17−19] For example, the 5-Fu:ZIF-8 host−guest complex had a loading capacity of 17.0%, and there was noncovalent interaction between 5-Fu:ZIF-8.[20] In β-CD-Na, the loading capacity was 23.0% compared to pure β-CD (16.7%).[6] Xu et al.[21] successfully obtained an HCFU host−guest complex with MOC-19; however, it was prone to hydrolysis.

Multiple methods have been employed for the structural characterization of the API:MOF complex, including thermal analysis,[22] nitrogen sorption,[23] X-ray methods,[24] and solid-
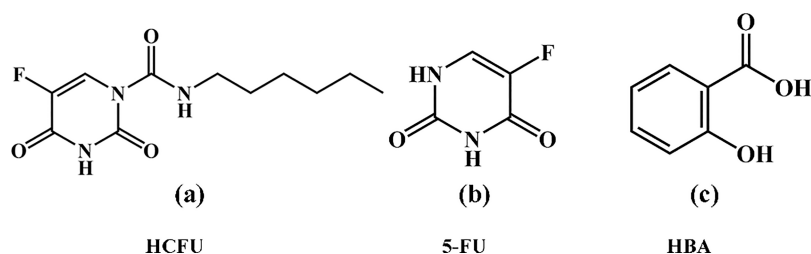
Figure 1. Molecular formulas with abbreviations of the selected API for the encapsulation process in this study.

state nuclear magnetic resonance (ssNMR).[24,25] Thermal analysis and nitrogen sorption offer both qualitative and quantitative insights about the bulk structural and thermodynamic properties of complex materials.[22,23] Powder X-ray diffraction (PXRD) is the usual method of choice for the investigation of structural properties, but it falls short of providing information at the atomic level about host–guest complex interactions without the single-crystal data.[21] An attractive alternative is ssNMR spectroscopy. This method can provide valuable information about the structural and dynamical properties of molecules at the atomic level regardless of their amorphous state.[25,26]

In this study, we aim to overcome these drawbacks by creating new API-encapsulated products within newly obtained γCD-K-5 and γCD-K-6 MOFs. We will characterize the loading capabilities of selected APIs with γCD-K MOFs[27] using various encapsulation protocols and study the API release processes for the obtained host–guest complexes. Additionally, we characterize the structures of the obtained complexes with various physical methods and *in vitro* and *in vivo* tests in cells.

■ MATERIALS AND METHODS

Materials. HCFU was purchased from BioNet, UK, and 5-FU was received as a gift from JSC Grindex. HBA, potassium carbonate, potassium iodide, and methanol were commercially available and used without further purification.

Equipment. The PXRD patterns were measured at ambient temperature on a D8 Advance (Bruker) diffractometer using copper radiation (CuKα) at a wavelength of 1.54180 Å, equipped with a LynxEye position-sensitive detector. The tube voltage and current were set to 40 kV and 40 mA, respectively. The divergence slit was set at 0.6 mm, and the antiscatter slit was set at 8.0 mm. The diffraction patterns were recorded using 0.2 s/0.02° scanning speed from 3° to 35° on the 2Θ scale.

Differential scanning calorimetry/thermogravimetric (DSC/TG) analyses were performed on a TGA/DSC2 apparatus (Mettler Toledo) using open 100 μL aluminum pans. Samples with a mass of 3–10 mg were heated under a nitrogen atmosphere (flow rate, 100 ± 10 mL min^{-1}) at a temperature range of 25–450 °C (heating rate, 10 °C min^{-1}).

Liquid chromatography–mass spectrometry (LC-MS) analysis was performed using a Waters Acquity UPLC H-class instrument equipped with an SQ Detector 2 mass detector system. The chromatographic column was an Acquity UPLC BEH-C18 2.1 × 50 mm, 1.7 μm. The eluent was acetonitrile and 0.1% formic acid–water solution in a ratio from 10:90 to 95:5. The flow rate was 0.5 mL min^{-1}. The mass spectrum was detected in negative mode (ESI$^-$). The second detector was a photodiode array (PDA) (200 to 300 nm).

Synthesis of MOFs. For γ-CD-K-5, γ-CD (648 mg, 0.5 mmol) and K$_2$CO$_3$ (1104 mg, 8 mmol) were dissolved in H$_2$O (10 mL). The obtained solution was stirred for 30 min at RT, and then MeOH (12 mL) was added. The precipitate was filtered and washed several times with MeOH. The obtained precipitate was dried at RT (21−25 °C).

For γ-CD-K-6, γ-CD (648 mg, 0.5 mmol) and KI (1328 mg, 8 mmol) were dissolved in H$_2$O (10 mL). The obtained solution was stirred for 30 min at RT, and MeOH (30−50 mL) was added to the water solution until precipitation started. The precipitate was filtered and washed several times with MeOH. The obtained precipitate was dried at RT (21−25 °C).

Characterization of MOFs. We selected two newly obtained MOFs as drug delivery systems to test their ability to encapsulate API on the structure. All selected MOF PXRD patterns can be seen in Figure S1, and TG/DSC results can be seen in Figure S2. Detailed description of thermal analyses is included in Section S1.

Incorporation of API with CD MOFs. *Method 1.* For the loading capacity of API in 24 h, a sample of API 20, 40, 60, and 80 mg was dissolved in 40 mL of methanol. The obtained solution was filtered, and 60 mg of dried γ-CD MOF was added. The suspension was filtered after 24 h, and the obtained solid was dried at RT (22 ± 2 °C) and, after that, weighed. The solvent of the experimental solution was evaporated. The solid after solvent evaporation was weighed. For the loading capacity of API 60 mg, a sample of API 60 mg was dissolved in 40 mL of methanol (prepared three identical samples). The obtained solution was filtered. After that, 60 mg of dried CD MOF was added. The suspension was filtered after 24, 48, and 72 h, and the obtained solid was dried at RT (22 ± 2 °C) and weighed. The solvent of the experiment solution was evaporated. The solid was weighed after solvent evaporation, and PXRD was recorded.

Method 2. A sample of API 20, 40, and 60 mg was dissolved in 40 mL of methanol. The obtained solution was filtered, and 60 mg of dried CD MOF was added. The solvent was evaporated using rotary evaporators at 200 mbar pressure. The water bath temperature was 40 ± 2 °C.

The actual API amount in CD MOF was determined from element analyses (see Table S1).

All of the obtained solids were characterized by PXRD.

Stability Testing of the Encapsulation Product. All obtained encapsulation products in the experiment with γ-CD-K-5 were stored at RT (22 ± 2 °C) and RH 30 ± 5% for 1 month. After that, PXRD was recorded and analyzed (Section S7).

Calibration of HPLC. All API (active pharmaceutical ingredient) calibration assays were analyzed by high-performance liquid chromatography at a range of API concentrations

(0.25, 0.5, and 1 mg/mL in methanol). The retention time of API was determined by analyzing the pure substance.

HCFU found, m/z: 281.01 $C_{24}H_{13}Cl_3N_7$. Calculated, m/z: 256.10.

5-FU found, m/z: 128.94 $[M - H]^-$ $C_4H_3FN_2O_2$. Calculated, m/z: 129.01.

HBA found, m/z: 136.93 $[M - H]^-$ $C_7H_6O_3$. Calculated, m/z: 137.02.

The calibration curve is shown in Figure S3.

Release Profiles. A predetermined quantity (30 mg) of accurately weighed API:CD MOF was submerged into 30 mL of preheated methanol maintained at 42 ± 2 °C under constant stirring at approximately 75 rpm. At predetermined time intervals (0.25, 0.5, 1, 2, 3, 5, 8, 12, 24, and 48 h), an aliquot of 1 mL was withdrawn. The aliquots were diluted 2× with the solvent and filtered by 0.2 μm syringe filter and analyzed using HPLC. The released percentage of all APIs was calculated according to eq 1:

$$R = \frac{\text{actual API released at any time (mg)}}{\text{amount of loaded with CD MOF (mg)}} \cdot 100 \quad (1)$$

We performed three experiments for every host−guest complex and calculated the average R factor and error.

^{13}C and ^{19}F Solid-State NMR Spectroscopy Experiments of APIs:γ-CD-K-5. All ssNMR spectra were acquired on an 18.8 T Bruker Advance III HD spectrometer equipped with a 3.2 mm H/F X probe at 16 kHz MAS frequency. The probe temperature was set to 0 °C. The ^{19}F spectra were acquired using a Hahn-echo sequence. The recycling delay was set to 5 s, and the acquisition time was 9 ms. All ^{1}H−^{13}C CP experiments were acquired using 3 s recycle delay and 17 ms acquisition time with 90 kHz ^{1}H SPINAL64 decoupling. All spectra were processed, analyzed, and plotted using TopSpin 3.6.1 software.

Cytotoxicity In Vitro. The cells were cultured at 37 °C in 75 cm² flasks in DMEM medium (for HepG2 and MO3.13) or EMEM medium (for BJ) supplemented with 10% heat-inactivated fetal bovine serum (FBS) and penicillin and streptomycin (P/S) under 5% CO_2. The medium was renewed twice a week, and cells were harvested when they obtained 80% of confluence. For experiments, the cells were seeded in 96- or 6-well plates in complete medium at a density of 2×10^5 cells/mL. The treatment was performed after 24 h. For the treatment, a serum-free medium was used. The cells were incubated with API for 24, 48, and 72 h to evaluate their toxicity. Inhibitory concentration (IC_{50}) was established for all APIs at each cell line. Then, at certain concentrations, APIs were co-incubated with CD for 72 h, and finally, based on the release profile, the toxicity of API:CD MOF carriers was evaluated.

Toxicity In Vivo in the Danio rerio Experimental Model. To determine the ecotoxicity of the compounds, the fish embryo toxicity (FET) test was performed on zebrafish (*Danio rerio*) according to the OECD Test Guideline 236. The collected embryos were transferred to a Petri dish with E3 medium (5 mM NaCl, 0.33 mM $MgCl_2$, 0.33 mM $CaCl_2$, and 0.17 mM KCl, pH 7.2) and then placed in 24-well plates, 5 embryos per well, 4 wells per group. Stock solutions of 5-FU, HCFU, and HBA were prepared in DMSO. In these experiments, three series of solutions with differing concentrations were employed, which were freshly prepared by dissolving stock solutions in the E3 solution each time directly

before addition to the wells. At the end of the exposure period (96 hpf, hours postfertilization), acute toxicity was determined based on a positive outcome in any of the four visual indicators of lethality, including the coagulation of fertilized eggs, lack of somite formation, lack of detachment of the tailbud from the yolk sac, and lack of heartbeat. The value of LD_{50} was calculated. Additionally, the fish from each group were monitored for the occurrence of developmental malformations. For the observations, a Discovery V8 stereooptical microscope and Zeiss hardware were used. A dose−response curve was generated using Prism 9 (GraphPad Software) by fitting a sigmoid curve model to the experimental data points. The concentrations of the compounds of interest causing 50% mortality (LD_{50}) of 96 hpf larvae of *D. rerio* were calculated.

■ RESULTS AND DISCUSSION

Incorporation of API with CD MOFs. The incorporation results of HCFU, 5-FU, and HBA into γ-CD-K-5 and γ-CD-K-6 are summarized in Tables 1 and 2. To determine the loading

Table 1. Obtained Results after Encapsulation Using γ-CD-K-5 as a Host[a]

method	another parameter	API		
		HCFU	5-FU	HBA
1A	20 mg	I + II + S	I + II	I
	40 mg	I + II + S	I + II	I
	60 mg	I + II + S	I + II	I
	80 mg	I + II + S	I + II	I
1B	24 h	I + sa. II	I + II	I + sa. II
	48 h	I + sa. II	I	I + sa. II
	72 h	I	I	I + sa. II
2	20 mg	II	II	II
	40 mg	II	II + 5FU	II + HBA
	80 mg	II + HCFU	II + 5FU	II + HBA

[a]I, encapsulation product 1; II, encapsulation product 2; S, HCFU another phase; sa, small amount of compound II (>5%).

Table 2. Obtained Results after Encapsulation Using γCD-K-6 as a Host[a]

method	another parameter	API		
		HCFU	5-FU	HBA
1A	20 mg	I	I	I
	40 mg	I	I	I
	60 mg	I + sa II	I	I
	80 mg	I + sa II	I	I
2	20 mg	II	I	II
	40 mg	II + S	A + 5-FU	II + HBA
	80 mg	II + S + 5-FU	A + 5-FU	II + HBA

[a]I, encapsulation product 1 (ZUGDIR[28]); II, encapsulation product 2; S, HCFU another phase; A, amorphous; sa, small amount of the compound (>5%).

efficiencies of selected APIs in the chosen MOFs, we applied two encapsulation protocols: (1) at 24 h using 20, 40, 60, and 80 mg of HCFU, 5-FU, or HBA and (2) using 60 mg of HCFU, 5-FU, or HBA, which can be reached on 72 h. All collected PXRD patterns are shown in Figures S4−S18.

The data shown in Table 1 indicate that all selected encapsulation experiments of APIs with γ-CD-K-5 resulted in two products. Using method 1, we mainly obtained product I
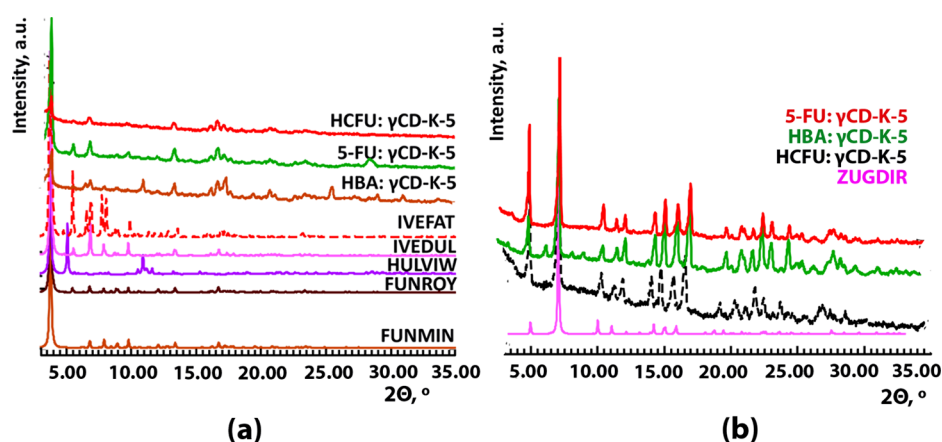
Figure 2. Comparison of PXRD patterns of encapsulation products with similar structural patterns in the published literature: (a) product II and (b) product I.

with the presence of product II; however, by method 2, we obtained product II only. The PXRD pattern (Figure 2b) of product I was similar to the published structure[28] of γ-CD-K (ZUGDIR). Compared to the ZUGDIR phase pattern, in the pattern of product I, the first peak intensity was higher and the second peak was slightly shifted at 7.24° on a 2θ scale for all encapsulated products (Figure 2b). This change can be attributed to host–guest molecular interactions upon complexation. Using encapsulation method 1, the starting phases remained in the solution after filtration of the product. Meanwhile, for encapsulation method 2, the solution was evaporated, and if the API was not completely encapsulated in the MOF, it appeared as an impurity in the final product (shown in Table 1). The MOF peaks were not present in the final solid pattern (shown in Figure 2). This indicated the structural instability of the selected γCD-K-5 during the encapsulation process, leading to the rearrangement of CD molecules with potassium ions. The phase transition occurred from pure γCD-K-5 to the γCD-K α phase without API under the experimental condition (MOF stability results can be seen in Figures S19 and S20). In samples containing HCFU (see Tables 1 and 2), another phase occurred after using encapsulation method 1.

The data shown in Table 2 indicated two encapsulation products for all APIs with γ-CD-K-6. API remains in the final product due to incomplete encapsulation using method 2, which required maximum loading mass values of 40 mg for HCFU and 20 mg for 5-FU and HBA. The same trend was observed in the γCD-K-5 case (Table 1).

Interestingly, both γCD-K-5 and γCD-K-6 rearranged to the same phases during the encapsulation process (Tables 1 and 2). This could be attributed to structural differences in the initial MOF structures; specifically, γCD-K-6 had a more densely packed structure compered to γCD-K-5, while γCD-K-5's structure is similar to that of ZUGDIR.[28]

The pure γ-CD-K-6 remained stable under experimental conditions. Elemental and XRD analyses confirmed that the MOF structure was preserved due to the presence of potassium ions in the sample (Table S1). The largest loading capacity was reached with method 2 (Table S1). We note here that the experimentally determined loading capacities of HBA and 5-FU in γCD-K- 5 were higher compared to the theoretically possible value. This might be due to the presence of additional water and methanol molecules in the starting MOF structure. Consequently, there could be an error in the weighted mass of

the reactants, leading to an increase in the overall weighted mass of MOFs.

All solids after MeOH evaporation were weighed (see Table S2) and analyzed with PXRD (method 1B sample). As can be seen from the PXRD data (see Figures S33−S35), the HCFU solid presented 5-FU, indicating possible hydrolyzation under the encapsulation conditions. However, there is no confidence that it occurs during impregnation in MOFs, as hydrolyzation can also occur during the evaporation process. If we analyze the loading efficiency from the remaining solid in the MeOH solvent, then for HBA, mass did not change after 48 h, but for HCFU and 5-FU, it did not change after 72 h. These changes in mass revealed that the maximum HBA encapsulation can be reached after 24 h, while for HCFU and 5-FU, it can be reached after 72 h. The highest loading capacity according to elemental analysis data was for HBA (24%, Table S1).

Summarizing the encapsulation results, we demonstrated the possibility to obtain two products: products I and II. PXRD data confirmed the structural similarity of product I to the structure of ZUGDIR (Figure 2b).[28] For product II, the structure was similar to several structures of FUNMIN,[29] FUNROY,[29] HULVIW,[30] IVEDUL, and IVEFAT[31] molecules (Figure 2a).

In general, based on PXRD data, the pattern of product I was more similar to the structures published in the literature compared to the product's II pattern. The PXRD pattern of the HBA:γCD-K-5 complex is more comparable to the IVEFAT structure pattern (Figure 2a). However, the patterns for HCFU:γCD-K-5 and 5-FU:γCD-K-5 complexes consisted of a combination of the two HULVIW and IVEDUL structure patterns (Figure 2a).

Stability Testing of Encapsulation Products. *Under Ambient Conditions.* The API encapsulation products with γCD-K-5 were selected for stability testing using PXRD patterns recorded before and after 1 month of storage at RT (22 ± 2 °C) and RH 30 ± 5%. All obtained results are shown in Section S7.

All encapsulation products that were obtained by method 1A exhibited decreased crystallinity after being stored under ambient conditions for 1 month (see Figures S21−S23). The encapsulation products that were obtained using methods 1B and 2 showed no major changes in the PXRD patterns (see Section S7). Hence, under these ambient conditions, the samples were stable. Minor changes were observed for 5-FU (Figure 3). In the 5-FU encapsulated complex, even after 1
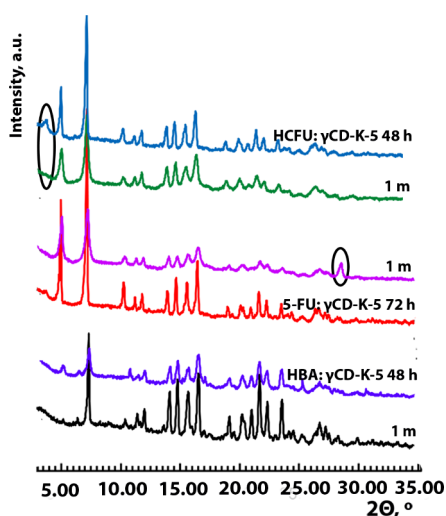
Figure 3. PXRD patterns of encapsulation products (using γCD-K-5 in method 1B) were stored at RT for 1 month (m, month).

month (compare to the initial sample), a peak at the 28° 2θ scale for neat 5-FU was detected. No other differences in PXRD patterns were observed. No free APIs for the HCFU and HBA complex were detected, and only some small insignificant changes were seen. These data indicated the lower stability of 5-FU:γCD-K-5 complexes compared to that of HCFU:γCD-K-5 and HBA:γCD-K-5.

DSC/TG Result. The host−guest complexes of API:CD MOF were characterized by differential scanning calorimetry (DSC) and thermogravimetric analysis (TGA). Summarized results can be seen in Section S12.

The DSC/TG data (see Figure S39) suggested that the data for encapsulation products and pure MOFs (γCD-K-5) were similar, with only minor differences detected. Previously, the DSC curve for neat 5-FU displayed a sharp single melting peak at 285.06 °C, followed by product degradation.[32] HBA exhibited a sharp endothermic (melting) peak at 160 °C,[33] but HCFU displayed a sharp endothermic peak at 110 °C.[34] These sharp peaks were not detected for encapsulation products (see Section S12).

The DSC curves of the encapsulation products also showed no distinct effects, but some samples showed weak endothermic effects before degradation.

The origins of mass loss can be divided into two parts: first, mass lost (5−10%) occurred at the beginning before reaching 100 °C temperature; probably, the water and methanol molecules in the channel or absorbed in surfaces vaporized. Second, a degradation mass change was observed before reaching 300 °C, but compared to a single γCD-K-5, this process occurred at higher temperature for all analyzed host−guest complex samples. Therefore, the encapsulation samples were more stable compared to free γCD-K-5.

Release Profiles. The calibration curve for HCFU, 5-FU, and HBA is shown in Figure S3. For the release experiment, the encapsulation products were obtained by using method 2. In this experiment, γCD-K-5 as the host was selected for the release process due to the higher loading capacity of the API, as determined from the elemental analysis (see Section S2).

The release profile (shown in Figure 4) exhibited a two-stage process for HBA and 5-FU:γCD-K-5. In the first stage, the release rates for HBA:γCD-K-5 and 5-Fu:γCD-K-5 were around 50% within the first 2 h. The second stage of HBA release from the HBA:γCD-K-5 complex occurred slowly, reaching only 61% within 100 h; however, 5-FU release from the complex reached almost 95% within 100 h.

A different pattern was observed for HCFU (Figure 4a). This was due to decomposition in the release process, during which HCFU:γCD-K-5 was possibly detected by HPLC with around 10% releases within 0.5 h, and then it was decomposed. The calculated possible release amount for HCFU from the complex from the decomposed compound was around 25% within 2 h (see Figure 4a). It was lower than those of 5-FU and HBA. These data indicated that the API was encapsulated inside the complex HCFU:γCD-K-5. However, if the release occurs, then decomposition follows anyway. This was a reason to avoid the HCFU complex's hydrolysis under unsuitable conditions for these APIs.

Detection of Possible Guest−Host Complex Interaction Using the ssNMR Method. Multidimensional ssNMR spectroscopy at the magic angle spinning (MAS) regime is a powerful technique to study the molecular structure and interactions for guest−host types of complexes at the
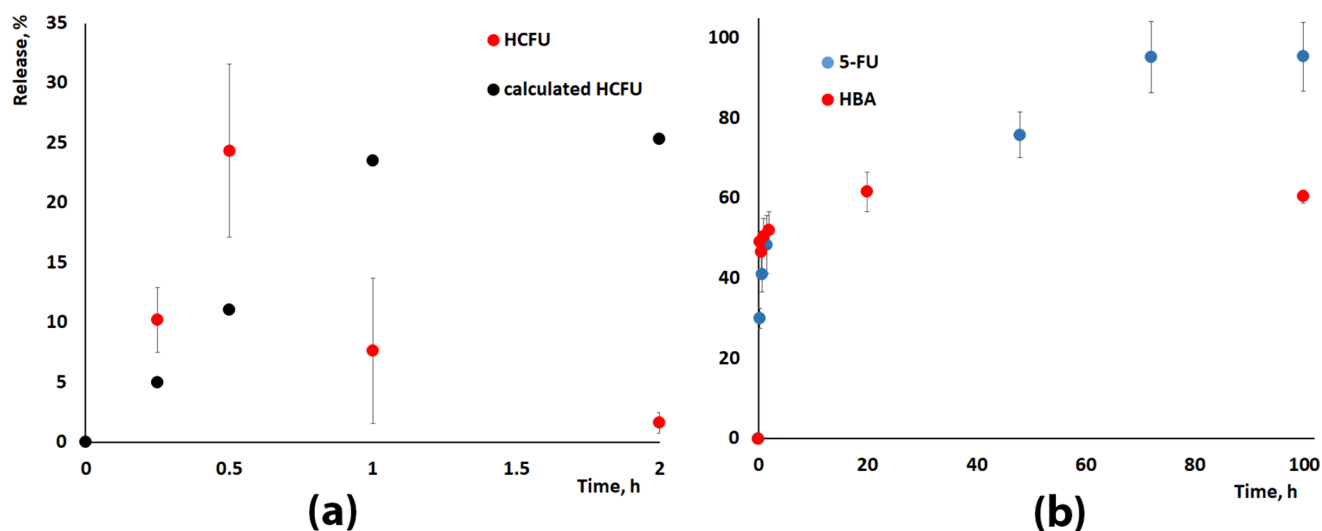

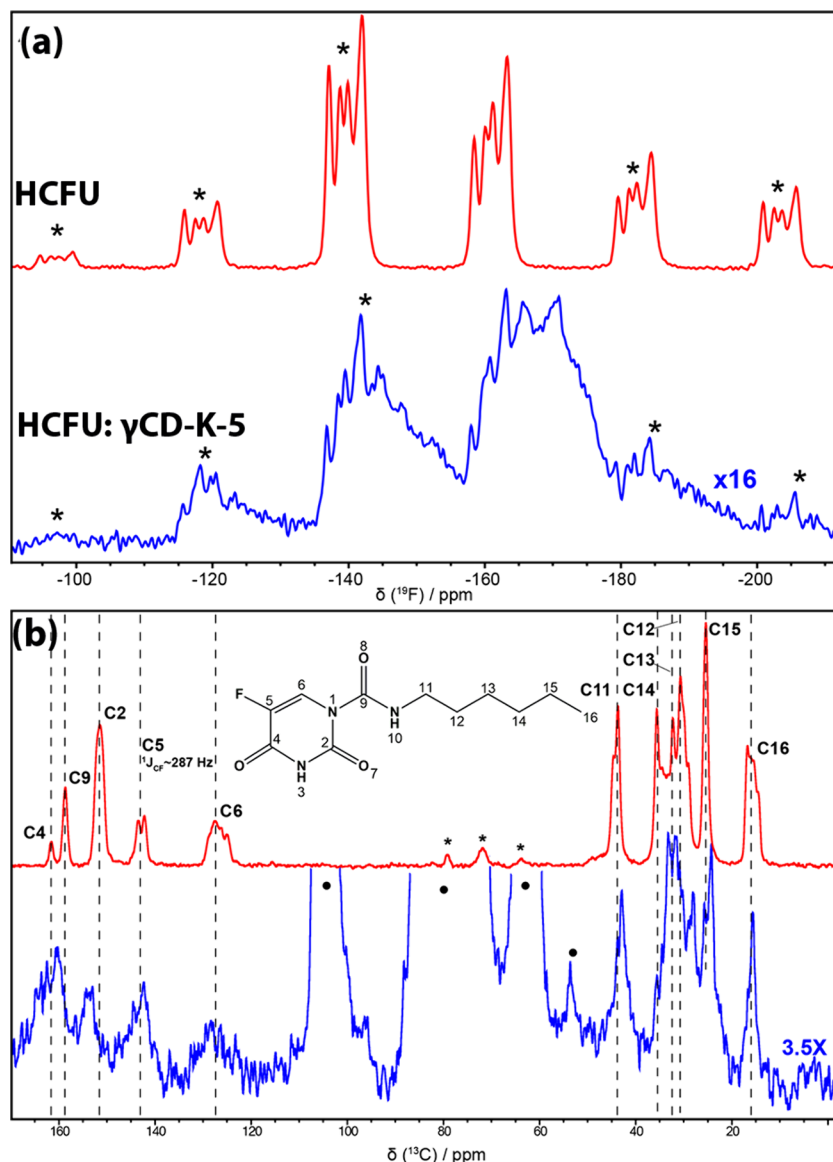**Figure 4.** API release profile: (a) HCFU and (b) 5-FU and HBA.

Figure 5. ssNMR spectra of HCFU (red) and HFCU:γCD-K-5 complex (blue). (a) ^{19}F HE and (b) ^{1}H$-^{13}$C CP. The molecular structure with corresponding carbon numbering is shown in panel (b). The MAS side bands in both spectra are indicated with an asterisk (*). In the ^{13}C spectrum, the peaks arising from γCD-K-5 are indicated with a solid circle.

atomic level.[35] In this study, we utilized 1D ^{1}H$-^{13}$C cross-polarization (CP) and ^{19}F Hahn-echo (HE) ssNMR experiments to study HCFU, FU, and HBA complexation with γCD-K-5. Both ^{13}C and ^{19}F chemical shifts are highly sensitive reporters for molecular interactions in ssNMR spectra.[36,37] Encapsulation products obtained by method 1A with γCD-K-5 were selected for the ssNMR experiments.

In the ^{19}F spectrum (Figure 5a and see Table S4), we observed 4 chemical shifts with similar intensities for a crystalline HCFU. This could indicate 4 molecules per 1 asymmetric unit in a crystalline cell. In the ^{1}H$-^{13}$C CP spectrum (Figure 5a), we assigned all ^{13}C chemical shifts for HCFU. The C5 resonance appeared as a doublet with $^{1}J_{CF}$ coupling of 283 Hz. The C6 peak was broad, possibly due to the peak overlap originating from differently oriented molecules or structural disorders. Other peaks from the pyridine ring exhibited single resonances. The shift for C11 in the aliphatic tail also exhibited 2 resonances, while C12, C13, C14, and C16 peaks displayed several overlapping peaks.

In the formed complex, the aliphatic tail could remain outside the cavity of γCD-K-5 and is affected by structural disorder, resulting in multiple peaks per aliphatic carbons. The inclusion of HCFU in γCD-K-5 resulted in severe reduction of peak intensities in ^{19}F and ^{1}H$-^{13}$C CP spectra (Figure 6). This is related to ~10% of HCFU incorporation in γCD-K-5 from elemental analysis (see Table S1). Additionally, in both ^{19}F and ^{13}C spectra (Figure 6), we observed severe line broadening and chemical shift perturbations (CSPs). Notably, both effects were also observed for ^{13}C peaks for apo and bound forms of γCD-K-5 (the ^{1}H$-^{13}$C CP spectral overlay is shown in Figure S36, and chemical shifts are listed in Table S5). Thus, both line-broadening effects and CSPs in ssNMR spectra indicated the formation of a host–guest complex between HCFU and γCD-K-5.

In the ^{19}F ssNMR spectrum of the triclinic 5-FU powder (shown in Figure 6a), we distinguished 4 peaks. Viger-Gravel et al.[38] observed, under low temperature conditions (−163 °C), two resonances with the similar chemical shifts for the
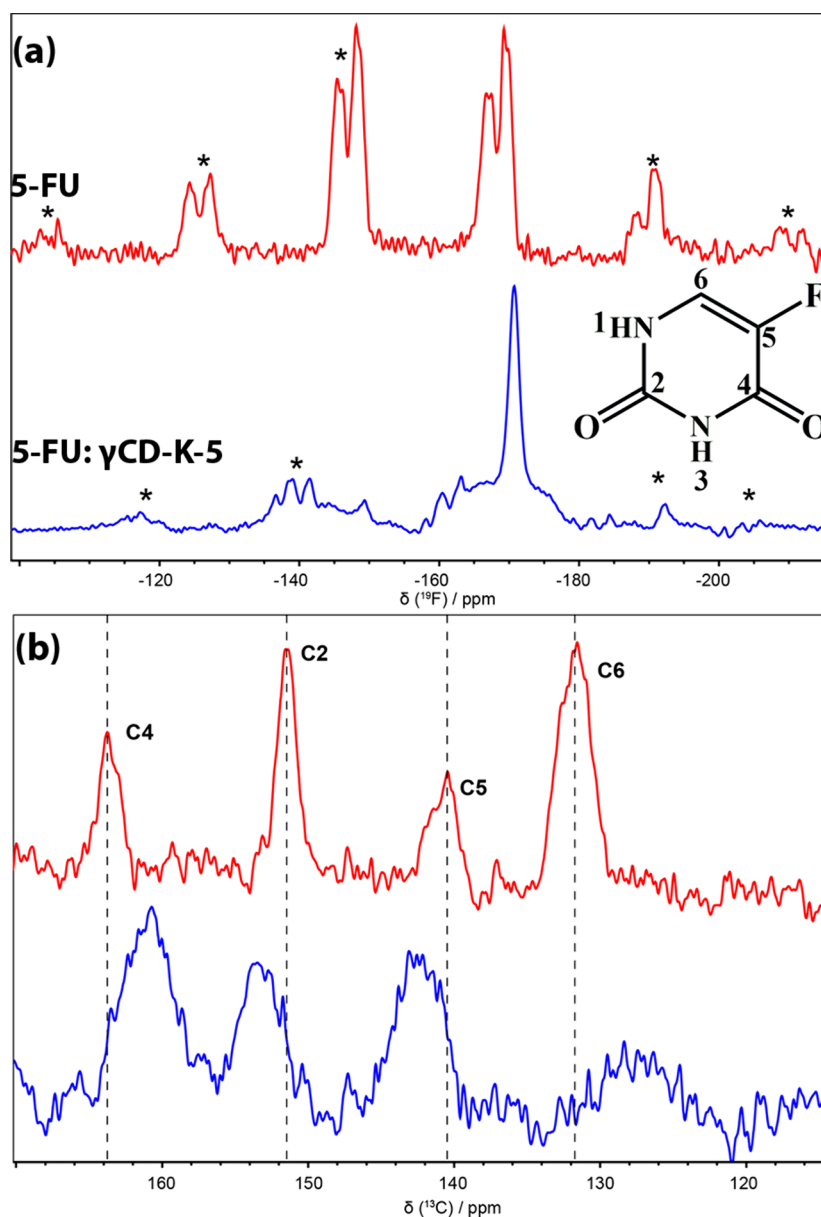
Figure 6. ssNMR spectra of 5-FU (red) and 5-Fu:γCD-K-5 complex (blue). (a) ^{19}F HE and (b) ^{1}H−^{13}C CP. The molecular structure with corresponding carbon numbering is shown. The MAS side bands in ^{19}F spectra are indicated with an asterisk (*).

same 5-FU crystalline form. Compared to RT data, often the linewidths in ssNMR spectra at cryogenic temperatures are broadened, resulting in peak overlapping. Also, reduction of peak intensities (in both ^{19}F and ^{13}C spectra) was observed, corresponding to only 6% (Table S1) of 5-Fu incorporation into γCD-K-5. The inclusion of 5-FU into γCD-K-5 led to severe line broadening for the upfield ^{19}F resonance at −167.1 ppm (Figure 6a). Previously, the ^{19}F line-broadening effects were also observed for the sample in which 5-Fu was mixed with an excipient matrix of cellulose.[38] Additionally, the other ^{19}F 5-Fu peak (at −169.5 ppm) exhibited a CSP of −1.2 ppm (Figure 7a and Table S4).

Based on the previous ^{13}C ssNMR assignments,[32] we identified all ^{13}C peaks of 5-FU (Figure 6B and Table S4). Compared to HCFU, the resolution in the ^{1}H−^{13}C CP spectrum for 5-FU was not sufficient to measure the $^1J_{CF}$ coupling for the C5 carbon. In the 5-FU:γCD-K-5 complex, all ^{13}C resonances from 5-FU exhibited significant CSP (Figure

6B and Table S4). The C4 (−3 ppm) and C6 (−4.0 ppm) peaks shifted upfield, while C2 (+2.4 ppm) and C5 (+2.4 ppm) peaks shifted downfield. Also, the ^{13}C linewidths for the complex had notably broadened, furthermore confirming the possible 5-FU molecule incorporation into γ-CD-K-5.

The ssNMR ^{13}C chemical shifts for HBA were previously reported,[39] and we observed similar chemical shifts for our HBA sample (Figure 7 and Table S6). Single resonances for all of the peaks indicated one molecule per asymmetric unit. Upon the addition of γCD-K-5, similar to HCFU and 5-FU, we monitored CSPs and line-broadening effects. Additionally, all ^{13}C resonances exhibited a reduction in peak intensities due to ~16% of HBA incorporation (SI Table S1). Substantial upfield and downfield CSPs were found for C1, C3, C4, and C7 resonances, while those for C5 and C6 remained the same. Due to severe line-broadening effects, the precise evaluation of CSP was not possible. Moreover, for the HBA:γCD-K-5 complex, C1 and C2 peaks were broadened beyond the
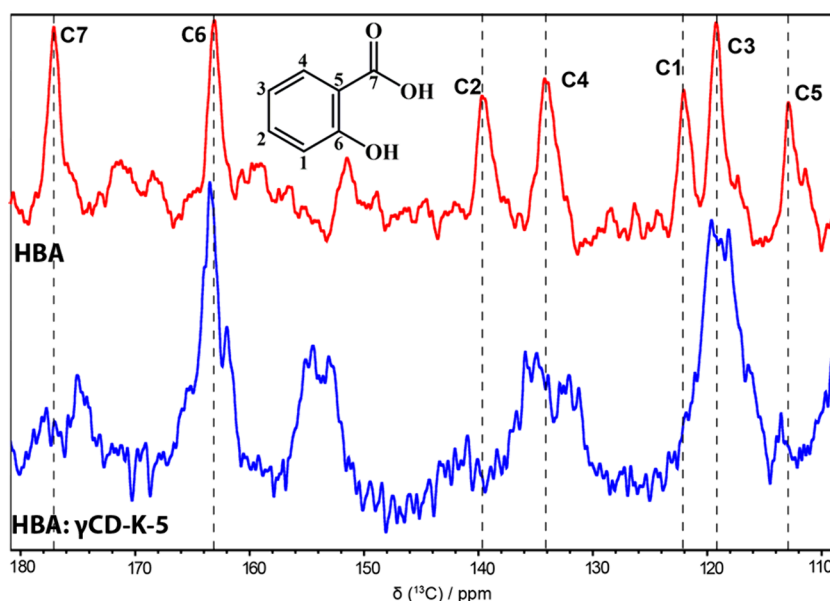
Figure 7. $^1H-^{13}C$ CP ssNMR spectra of HBA (red) and HBA:γ-CD-K-5 complex (blue). The molecular structure with the corresponding carbon numbering scheme is shown on top.

detection limit (Figure 7). This could indicate the possible encapsulation process through the moieties spatially in close proximity to the acidic group within HBA. Previously, for HBA encapsulated in PEG/γCD-polypseudorotaxa, similar changes were observed in the ssNMR $^1H-^{13}C$ CP spectrum.[39]

Overall, ssNMR spectroscopy revealed the significant changes in 1D ^{19}F- and ^{13}C-detected ssNMR spectra, further confirming the encapsulation of 3 APIs (5-FU, HCFU, and HBA) into γ-CD-K-5. Further, the application of faster MAS rates and simultaneous ^1H decoupling will improve resolution and sensitivity in fluorine-detected spectra.[40] Additionally, faster MAS rates (above 100 kHz) would enable the acquisition of highly resolved ^1H-detected multidimensional spectra even for heterogeneous samples.[41] This advancement would open a new avenue for more detailed structural information at the atomic level for amorphous complexes.

Cytotoxicity *In Vitro* and Toxicity *In Vivo*. We conducted cytotoxicity studies using HepG2 (ATCC, HB-8065), a human liver cancer cell line, as the cellular model for hepatotoxicity and M03.13 (Tebubio, CLU301-P), an immortal human−human hybrid cell line that expresses phenotypic characteristics of primary oligodendrocytes, as the *in vitro* model of neurotoxicity. Our study (see Figure S37) has revealed a neurotoxic effect of the studied APIs that is higher than the hepatotoxic effect. Both neurotoxicity and hepatotoxicity were time-dependent, with the highest toxicity observed after 72 h of intoxication.

Then, we explored the effects of CDs and MOFs on cytotoxicity using the M03.13 cell line. Our study proved slight cytoprotective effects (Figure 8a) of all CDs, which were the highest for βCD complexes with all APIs (measured at the dose of 25 μg/mL). Notably, the cytoprotective effect was more pronounced when APIs were combined with MOFs (API:γCD-K-5) (Figure 8b). A statistically significant increase in viability was observed between 72 h-long intoxication of the M03.13 cell line with API alone compared to API:γCD-K-5 at the same dose of 25 μg/mL. In the case of the highest dose, 50 μg/mL, cell survival was only in the case of API:γCD-K-5 application.

In the next stage of the experiment, we assessed the toxicity of APIs *in vivo* using the *D. rerio* experimental model. We compared the ecotoxicity of APIs alone or in combination with CDs (see Figure S38). Our findings proved a protective role of CDs against API toxicity, with the highest protective effect of βCD for 5-FU and HBA and γCD for HCFU. Additionally, for HBA at a dose of 50 μg/mL, both βCD and γCD demonstrated protective effects against the occurrence of developmental malformations. Similarly, for 5-FU at doses of 50 and 75 μg/mL, all CDs exhibited protective effects against the occurrence of developmental malformations. These malformations included pericardial edema (PE), scoliosis (S), and tail autophagy (TA).

Finally, we compared all CDs, pure MOFs, and loaded MOFs (API:MOF) using the *D. rerio* experimental model for toxicity (see Table S7). Our result proved the safety of CDs, pure γCD, γCD-K-5, and γCD-K-6 MOFs as well as for 5-FU:γCD-K-5. The most toxic appeared to be HBA:γCD-K-5 at higher dose (2 mg/3 mL), while application of HCFU:γCD-K-5 stopped hatching.

■ CONCLUSIONS

The selected APIs, the anticancer drugs HCFU and 5-FU and with the skin treatment drug HBA, were successfully encapsulated in the selected newly synthesized MOFs γCD-K-5 and γCD-K-6. High loading capacity values (9−30 wt %) were achieved using different encapsulation methodologies. As a result, we obtained different host−guest complexes—products I and II with different encapsulation effectiveness. Although the primary MOF structure was unstable, leading to structural rearrangement, this did not hinder the formation of the guest−host system. The possible interaction and complex formation were confirmed by ssNMR spectroscopy, which showed to be an alternative tool to PXRD in the absence of single-crystal data. *In vitro* and *in vivo* studies proved the protective role of CDs and CD-based MOFs against normal cells as well as in the model organism of *D. rerio*. Additionally, our studies proved γCD-K-5 (pure MOF) as the most protective and safe option for drug encapsulation to decrease
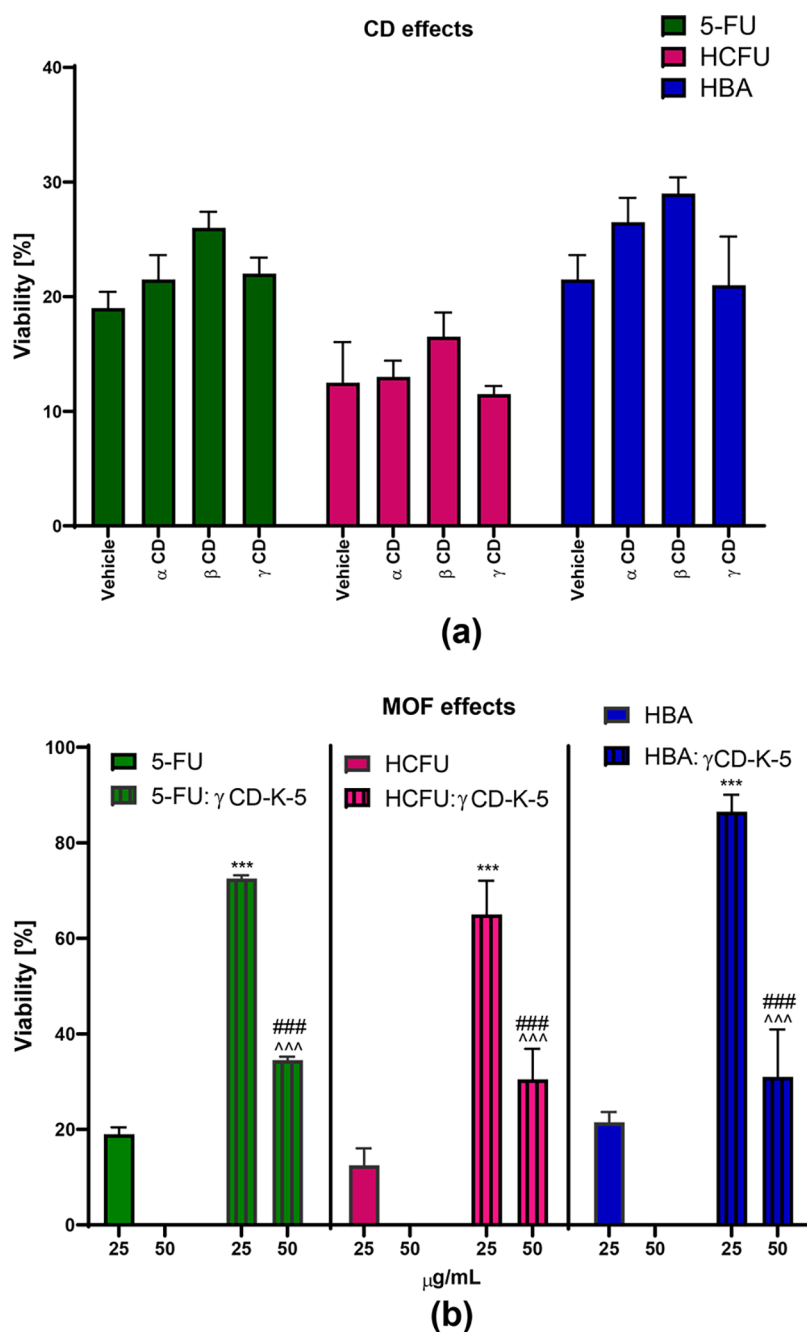
Figure 8. (a) Combined API and CD cytotoxicity and (b) comparison of the cytotoxicity of free API versus API:γCD-K-5. ***$p < 0.001$ API (25 μg/mL) vs API:γCD-K-5 (25 μg/mL), ^^^$p < 0.05$ API (50 μg/mL) vs API:γCD-K-5 (50 μg/mL), and ###$p < 0.001$ API:γCD-K-5 (25 μg/mL) vs API:γCD-K-5 (50 μg/mL), Sidak's multiple comparison test.

the toxicity level against normal cells. Based on our finding, we anticipate that the newly obtained MOFs—γCD-K-5 and γCD-K-6 complexes—can be further explored as potential candidates for a novel drug delivery system.

■ ASSOCIATED CONTENT

Ⓢ Supporting Information

The Supporting Information is available free of charge at https://pubs.acs.org/doi/10.1021/acsomega.3c06745.

Characterization of used γCD-K MOF-obtained PXRD and DSC/TG data, elemental analysis-obtained results, encapsulation-obtained product mass and precipitate mass after reaction solvent evaporation, calibration of

HPLC analyses, obtained PXRD patterns after encapsulation experiments, stability PXRD patterns of the MOFs under experimental condition without APIs using method 2, stability experiment PXRD pattern of the encapsulation product after 1 month at RT, PXRD patterns of the solid after encapsulation reaction solvent evaporation, WDXRF method experimental condition, ^{13}C and ^{19}F ssNMR chemical shifts, cytotoxicity *in vitro* and toxicity *in vivo* data, and host−guest complex DSC/TG results (PDF)

■ AUTHOR INFORMATION

Corresponding Author

Kristīne Krūkle-Bērziņa − *Latvian Institute of Organic Synthesis, Riga LV-1006, Latvia;* ● orcid.org/0000-0003-0899-3927; Email: kkberzina@osi.lv

Authors

Alons Lends − *Latvian Institute of Organic Synthesis, Riga LV-1006, Latvia*

Anna Boguszewska-Czubara − *Department of Medical Chemistry, Medical University of Lublin, Lublin 20-093, Poland*

Complete contact information is available at:
https://pubs.acs.org/10.1021/acsomega.3c06745

Notes

The authors declare no competing financial interest.

■ REFERENCES

(1) Zhong, L.; Li, Y.; Xiong, L.; Wang, W.; Wu, M.; Yuan, T.; Yang, W.; Tian, C.; Miao, Z.; Wang, T.; Yang, S. Small Molecules in Targeted Cancer Therapy: Advances, Challenges, and Future Perspectives. *Signal Transduct. Target. Ther.* **2021**, *6* (1), 201.

(2) Palumbo, M. O.; Kavan, P.; Miller, W. H. J.; Panasci, L.; Assouline, S.; Johnson, N.; Cohen, V.; Patenaude, F.; Pollak, M.; Jagoe, R. T.; Batist, G. Systemic Cancer Therapy: Achievements and Challenges That Lie Ahead. *Front. Pharmacol.* **2013**, *4*, 57.

(3) Adepu, S.; Ramakrishna, S. Controlled Drug Delivery Systems: Current Status and Future Directions. *Molecules* **2021**, *26* (19), 5905.

(4) Xin, Y.; Yin, M.; Zhao, L.; Meng, F.; Luo, L. Recent Progress on Nanoparticle-Based Drug Delivery Systems for Cancer Therapy. *Cancer Biol. Med.* **2017**, *14* (3), 228−241.

(5) Li, H.; Lv, N.; Li, X.; Liu, B.; Feng, J.; Ren, X.; Guo, T.; Chen, D.; Fraser Stoddart, J.; Gref, R.; Zhang, J. Composite CD-MOF Nanocrystals-Containing Microspheres for Sustained Drug Delivery. *Nanoscale* **2017**, *9* (22), 7454−7463.

(6) Han, Y.; Liu, W.; Huang, J.; Qiu, S.; Zhong, H.; Liu, D.; Liu, J. Cyclodextrin-Based Metal-Organic Frameworks (CD-MOFs) in Pharmaceutics and Biomedicine. *Pharmaceutics* **2018**, *10* (4), 271.

(7) Sha, J.; Yang, X.; Sun, L.; Zhang, X.; Li, S.; Li, J.; Sheng, N. Unprecedented *α*-Cyclodextrin Metal-Organic Frameworks with Chirality: Structure and Drug Adsorptions. *Polyhedron* **2017**, *127*, 396−402.

(8) Zhao, R.; Zhu, B.; Xu, Y.; Yu, S.; Wang, W.; Liu, D.; Hu, J. Cyclodextrin-Based Metal-Organic Framework Materials: Classifications, Synthesis Strategies and Applications in Variegated Delivery Systems. *Carbohydr. Polym.* **2023**, *319*, No. 121198.

(9) Hamedi, A.; Anceschi, A.; Patrucco, A.; Hasanzadeh, M. A *γ*-Cyclodextrin-Based Metal-Organic Framework (*γ*-CD-MOF): A Review of Recent Advances for Drug Delivery Application. *J. Drug Target.* **2022**, *30* (4), 381−393.

(10) Uekama, K.; Hirayama, F. 38 - IMPROVEMENT OF DRUG PROPERTIES BY CYCLODEXTRINS. In *The Practice of Medicinal Chemistry* (Second ed.); Wermuth, C. G., Ed.; Academic Press: London, 2003; pp 649−673. DOI: 10.1016/B978-012744481-9/50042-8.

(11) Nguyen, H.; Awad, A.; Shabani, S.; Doan, N. Molecular Targeting of Acid Ceramidase in Glioblastoma: A Review of Its Role, Potential Treatment, and Challenges. *Pharmaceutics* **2018**, *10* (2), 45.

(12) Rider, B. J. 5 Fluorouracil. In *xPharm: The Comprehensive Pharmacology Reference*; Enna, S. J.; Bylund, D. B., Eds.; Elsevier: New York, 2007; pp 1−5.

(13) Ma, Y.; Wang, Y.; Xu, Z.; Wang, Y.; Fallon, J. K.; Liu, F. Extreme Low Dose of 5-Fluorouracil Reverses MDR in Cancer by Sensitizing Cancer Associated Fibroblasts and down-Regulating P-Gp. *PLoS One* **2017**, *12* (6), No. e0180023.

(14) Sampedro-Guerrero, J.; Vives-Peris, V.; Gomez-Cadenas, A.; Clausell-Terol, C. Improvement of Salicylic Acid Biological Effect through Its Encapsulation with Silica or Chitosan. *Int. J. Biol. Macromol.* **2022**, *199*, 108−120.

(15) Belsito, D.; Bickers, D.; Bruze, M.; Calow, P.; Greim, H.; Hanifin, J. M.; Rogers, A. E.; Saurat, J. H.; Sipes, I. G.; Tagami, H. A Toxicologic and Dermatologic Assessment of Salicylates When Used as Fragrance Ingredients. *Food Chem. Toxicol.* **2007**, *45* (1), S318−S361.

(16) Labib, R.; Bury, D.; Boisleve, F.; Eichenbaum, G.; Girard, S.; Naciff, J.; Leal, M.; Wong, J. A Kinetic-Based Safety Assessment of Consumer Exposure to Salicylic Acid from Cosmetic Products Demonstrates No Evidence of a Health Risk from Developmental Toxicity. *Regul. Toxicol. Pharmacol.* **2018**, *94*, 245−251.

(17) Rajkumar, T.; Kukkar, D.; Kim, K. H.; Sohn, J. R.; Deep, A. Cyclodextrin-Metal−Organic Framework (CD-MOF): From Synthesis to Applications. *J. Ind. Eng. Chem.* **2019**, *72*, 50−66.

(18) Yu, G.; Chen, X. Host-Guest Chemistry in Supramolecular Theranostics. *Theranostics* **2019**, *9* (11), 3041−3074, DOI: 10.7150/thno.31653.

(19) Gidwani, B.; Vyas, A. A Comprehensive Review on Cyclodextrin-Based Carriers for Delivery of Chemotherapeutic Cytotoxic Anticancer Drugs. *Biomed. Res. Int.* **2015**, *2015*, 1.

(20) Wang, Q.; Sun, Y.; Li, S.; Zhang, P.; Yao, Q. Synthesis and Modification of ZIF-8 and Its Application in Drug Delivery and Tumor Therapy. *RSC Adv.* **2020**, *10* (62), 37600−37620.

(21) Xu, W.; Qiu, Y.; He, S.; Peng, S.; Xie, B.; Zhong, M.; Jiang, T.; Liu, X.; Yin, W.; Jiang, J. Probing of the Supramolecular Interaction between Anti-Cancer Drug Carmofur and a Zn 4 L 4 Metal-Organic Cage in Acetonitrile. *Inorg. Chem. Commun.* **2018**, *87*, 24−26.

(22) Loganathan, S.; Valapa, R. B.; Mishra, R. K.; Pugazhenthi, G.; Thomas, S. Chapter 4 - Thermogravimetric Analysis for Characterization of Nanomaterials. In Thermal and Rheological Measurement Techniques for Nanomaterials Characterization; Thomas, S.; Thomas, R.; Zachariah, A. K.; Mishra, R. K., Eds.; *Micro Nano Technol.*; Elsevier, 2017; pp 67−108. DOI: 10.1016/B978-0-323-46139-9.00004-9.

(23) Ambroz, F.; Macdonald, T. J.; Martis, V.; Parkin, I. P. Evaluation of the BET Theory for the Characterization of Meso and Microporous MOFs. *Small. Methods* **2018**, *2* (11), 1800173.

(24) Ukmar, T.; Čendak, T.; Mazaj, M.; Kaučič, V.; Mali, G. Structural and Dynamical Properties of Indomethacin Molecules Embedded within the Mesopores of SBA-15: A Solid-State NMR View. *J. Phys. Chem. C* **2012**, *116* (4), 2662−2671.

(25) Porcino, M.; Li, X.; Gref, R.; Martineau-Corcos, C. Solid-State NMR Spectroscopy: A Key Tool to Unravel the Supramolecular Structure of Drug Delivery Systems. *Molecules* **2021**, *26* (14), 4142.

(26) Wong, Y. T. A.; Martins, V.; Lucier, B. E. G.; Huang, Y. Solid-State NMR Spectroscopy: A Powerful Technique to Directly Study Small Gas Molecules Adsorbed in Metal−Organic Frameworks. *Chem. − Eur. J.* **2019**, *25* (8), 1848−1853.

(27) Krūkle-Bērziņa, K.; Mishnev, A. Never-Ending Story: New Cyclodextrin-Based Metal−Organic Framework Crystal Structures Obtained Using Different Crystallization Methods. *ACS Omega* **2023**, *8* (50), 48221−48232.

(28) Krūkle-Bērziņa, K.; Belyakov, S.; Mishnev, A.; Shubin, K. Stability and Phase Transitions of Nontoxic *γ*-Cyclodextrin-K+ Metal-Organic Framework in Various Solvents. *Crystals* **2020**, *10* (1), 37.

(29) Shen, D.; Cooper, J. A.; Li, P.; Guo, Q.-H.; Cai, K.; Wang, X.; Wu, H.; Chen, H.; Zhang, L.; Jiao, Y.; Qiu, Y.; Stern, C. L.; Liu, Z.; Sue, A. C.-H.; Yang, Y.-W.; Alsubaie, F. M.; Farha, O. K.; Stoddart, J. F. Organic Counteranion Co-Assembly Strategy for the Formation of

γ-Cyclodextrin-Containing Hybrid Frameworks. *J. Am. Chem. Soc.* **2020**, *142* (4), 2042−2050.

(30) Yang, P.; Alshankiti, B.; Khashab, N. M. Intrinsically Porous Molecular Building Blocks for Metal Organic Frameworks Tailored by the Bridging Effect of Counter Cations. *CrystEngComm* **2020**, *22* (17), 2889−2894.

(31) Chen, X.-Y.; Chen, H.; Đorđević, L.; Guo, Q.-H.; Wu, H.; Wang, Y.; Zhang, L.; Jiao, Y.; Cai, K.; Chen, H.; Stern, C. L.; Stupp, S. I.; Snurr, R. Q.; Shen, D.; Stoddart, J. F. Selective Photodimerization in a Cyclodextrin Metal−Organic Framework. *J. Am. Chem. Soc.* **2021**, *143* (24), 9129−9139.

(32) Egodawatte, S.; Dominguez, S.; Larsen, S. C. Solvent Effects in the Development of a Drug Delivery System for 5-Fluorouracil Using Magnetic Mesoporous Silica Nanoparticles. *Microporous Mesoporous Mater.* **2017**, *237*, 108−116.

(33) Elbagerma, M. A.; Edwards, H. G. M.; Munshi, T.; Scowen, I. J. Identification of a New Co-Crystal of Salicylic Acid and Benzamide of Pharmaceutical Relevance. *Anal. Bioanal. Chem.* **2010**, *397* (1), 137−146.

(34) Bao, Y.; Li, S.; Liu, L.; Luan, Y.; Lin, G.; Shao, W. Carmofur-Loaded Pluronic P123 Polymeric Micelles: Preparation and Characterization. *J. Dispers. Sci. Technol.* **2012**, *33* (4), 617−621.

(35) Mazurek, A. H.; Szeleszczuk, Ł. A Review of Applications of Solid-State Nuclear Magnetic Resonance (SsNMR) for the Analysis of Cyclodextrin-Including Systems. *Int. J. Mol. Sci.* **2023**, *24* (4), 3648.

(36) Arrúa, E. C.; Ferreira, M. J. G.; Salomon, C. J.; Nunes, T. G. Elucidating the Guest-Host Interactions and Complex Formation of Praziquantel and Cyclodextrin Derivatives by 13C and 15N Solid-State NMR Spectroscopy. *Int. J. Pharm.* **2015**, *496* (2), 812−821.

(37) Du, Y.; Su, Y. 19F Solid-State NMR Characterization of Pharmaceutical Solids. *Solid State Nucl. Magn. Reson.* **2022**, *120*, No. 101796.

(38) Viger-Gravel, J.; Avalos, C. E.; Kubicki, D. J.; Gajan, D.; Lelli, M.; Ouari, O.; Lesage, A.; Emsley, L. 19 F Magic Angle Spinning Dynamic Nuclear Polarization Enhanced NMR Spectroscopy. *Angew. Chemie Int. Ed.* **2019**, *58* (22), 7249−7253.

(39) Higashi, K.; Ideura, S.; Waraya, H.; Moribe, K.; Yamamoto, K. Incorporation of Salicylic Acid Molecules into the Intermolecular Spaces of γ-Cyclodextrin-Polypseudorotaxane. *Cryst. Growth Des.* **2009**, *9* (10), 4243−4246.

(40) Quinn, C. M.; Zadorozhnyi, R.; Struppe, J.; Sergeyev, I. V.; Gronenborn, A. M.; Polenova, T. Fast 19F Magic-Angle Spinning Nuclear Magnetic Resonance for the Structural Characterization of Active Pharmaceutical Ingredients in Blockbuster Drugs. *Anal. Chem.* **2021**, *93* (38), 13029−13037.

(41) Nishiyama, Y.; Hou, G.; Agarwal, V.; Su, Y.; Ramamoorthy, A. Ultrafast Magic Angle Spinning Solid-State NMR Spectroscopy: Advances in Methodology and Applications. *Chem. Rev.* **2023**, *123* (3), 918−988.